Highly active nanocrystalline TiO_2 photoelectrodes

2008 Nanotechnology 19 115201

(http://iopscience.iop.org/0957-4484/19/11/115201)

Nanotechnology **19** (2008) 115201 (10pp) doi:10.1088/0957-4484/19/11/115201

Highly active nanocrystalline TiO_2 photoelectrodes

Tereza M Paronyan[1,2], A M Kechiantz[1,3] and M C Lin[1,4]

[1] Department of Applied Chemistry and Institute of Molecular Science, National Chiao Tung University, Hsinchu, Taiwan
[2] Institute for Physical Research, National Academy of Sciences of Armenia, Ashtarak-2, Armenia
[3] Institute of Radiophysics and Electronics, National Academy of Sciences of Armenia, Ashtarak-1, Armenia
[4] Department of Chemistry, Emory University, Atlanta, GA, USA

E-mail: tparonyan@mail.nctu.edu.tw and pantea@ipr.sci.am

Received 31 August 2007, in final form 9 January 2008
Published 18 February 2008
Online at stacks.iop.org/Nano/19/115201

Abstract

A simple method for the fabrication of highly photoactive nanocrystalline two-layer TiO_2 electrodes for solar cell applications is presented. Diluted titanium acetylacetonate has been used as a precursor for covering SnO_2:F (FTO) films with dense packed TiO_2 nanocrystallites. The nanoporous thick TiO_2 film follows the dense packed thin TiO_2 film as a second layer. For the latter, amorphous TiO_2 nanoparticles have been successfully synthesized by a sol–gel technique in an acidic environment with pH < 1 and hydrothermal growth at a temperature of 200 °C. The acidic nanoparticle gel was neutralized by basic ammonia and a TiO_2 gel of pH 5 was obtained; this pH value is higher than the recently reported value of 3.1 (Park *et al* 2005 *Adv. Mater.* **17** 2349–53). Highly interconnected, nanoporous, transparent and active TiO_2 films have been fabricated from the pH 5 gel. SEM, AFM and XRD analyses have been carried out for investigation of the crystal structure and the size of nanoparticles as well as the surface morphology of the films. Investigation of the photocurrent–voltage characteristics has shown improvement in cell performance along with the modification of the surface morphology, depending on pH of the TiO_2 gel. Increasing the pH of the gel from 2.1 to 5 enhanced the overall conversion efficiency of the dye-sensitized solar cells by approximately 30%. An energy conversion efficiency of 8.83% has been achieved for the cell (AM1.5, 100 $mWcm^{-2}$ simulated sunlight) compared to 6.61% efficiency in the absence of ammonia in the TiO_2 gel.

(Some figures in this article are in colour only in the electronic version)

1. Introduction

Photoactive nanocrystalline TiO_2 films are regarded as the basic component of dye-sensitized and quantum-dot-sensitized solar cells [1–4]. The fabrication procedure for TiO_2 electrodes includes synthesis of nanoparticles, deposition of nanoporous films composed of nanoparticles, and activation of the nanocrystalline films for dye absorption. The photocatalytic activity of nanocrystalline TiO_2 films strongly depends on the size and structure of the nanoparticles, on the interconnection between them as well as on the surface activity and porosity of the films.

Amorphous TiO_2 nanoparticles for solar cell applications are usually synthesized by a sol–gel technique either in an acid or a basic environment [5–7]. The size, the shape and the crystal structure of nanoparticles are controlled by the pH of the synthesis environment and by the temperature of hydrothermal growth (autoclaving) [8–13]. A concentrated gel composed of amorphous TiO_2 nanoparticles is deposited on transparent conductive substrates such as FTO and ITO (In_2O_3:SnO_2). Heat treatment at higher temperatures follows the deposition for both crystallization and interconnection of the TiO_2 nanoparticles.

The performance of the solar cell is significantly improved when the nanoparticles are better interconnected with each other [14–16]. The viscosity of the gel composed of particles has a direct influence on particle interconnection in the films fabricated from that gel. Organic binders are usually

added to increase the viscosity of the colloid solution in order to improve the interconnection of nanoparticles. As a consequence of this, difficulties have arisen in removing all the organic traces from the nanocrystalline films. However, the viscosity can be enhanced not only by adding binders, but also by increasing the pH of the colloid solution. It is known that slurry is most viscous at the point of zero charge (PZC) of its nanoparticles [17]. As the PZC of anatase TiO_2 is at pH 6.2 [19] by changing the pH of the TiO_2 gel close to this point, the gel will become more viscous. A photocurrent density of $J_{sc} = 7.06$ mA cm^{-2} and conversion efficiency of 3.52% have recently been achieved in dye-sensitized solar cells (DSSC) fabricated in this way at low temperatures from the colloid gel with pH 3.1 [18]. The authors increased the viscosity of TiO_2 gel by adding basic ammonia to the binder-free acidic gel. It has also been reported that further adding of ammonia to the colloid solution does not significantly increase the pH, and therefore the viscosity, of the slurry [18].

In this paper, we report on a new simplified method of fabrication of highly photoactive two-layer nanocrystalline TiO_2 electrodes. The method includes using diluted titanium acetylacetonate as a precursor for deposition of dense packed nanocrystalline thin TiO_2 films by spray pyrolysis. Afterwards the binder-free TiO_2 gel, pH 5, is deposited on the dense films by a doctor-blade technique. The pH value of 5 of the concentric gel was reached by modifying the environment of the sol to pH 0.95 before hydrothermal growth. Ammonia hydroxide was used to neutralize the acidic TiO_2 gel reaching a pH close to the anatase PZC. SEM, AFM and XRD analyses revealed that adding basic ammonia to the acidic gel has a significant influence on crystallization, interconnection and surface activity of TiO_2 nanoparticles. Analyzing the photocurrent–voltage characteristics of DSSC, we have come to the conclusion that ammonia improves interconnection of TiO_2 nanoparticles and increases the overall conversion efficiency of DSSCs by approximately 30% due to discharging the environment of nanoparticles. Though the proposed method has not been completely optimized yet, a conversion efficiency of 8.83% has already been achieved under illumination by simulated AM 1.5 solar light (100 mW cm^{-2}).

The developed technique simplifies the fabrication of highly active nanocrystalline TiO_2 photoelectrodes. It avoids some standard procedures of fabrication such as adding the binder, activating the surface of TiO_2 nanoparticles by treating films in the $TiCl_4$ aqueous solution, and immersing the hot electrodes into a dye solution.

2. Experimental details

2.1. Colloid synthesis

The amorphous TiO_2 nanoparticles were synthesized by the sol–gel method using titanium alkoxide as a titanium source [5, 6]. Titanium (IV) isopropoxide (Sigma-Aldrich, 97%) 37 ml in 10 ml 2-propanol (Fluka, 99.8%) was slowly dripped over 40 min into a stirred mixture of 80 ml glacial acetic acid containing 250 ml of deionized water cooled in an ice bath. 0.06 M HNO_3 (Fluka, 65%) was added dropwise to the white resultant under stirring. The slurry became a translucent blue-white liquid with a pH between 0.95 and 0.98 measured by pH meter (Suttex Microprocessor SP2200) at a temperature of 21 °C. To complete the peptization, the translucent liquid was heated at 80 °C in an oil bath for 8 h under stirring. The resultant suspensions were treated hydrothermally at 200 °C for 12 h. These autoclaving conditions gave rise to the average nanoparticle size of 20 nm. After autoclaving, the pH of the colloid solution was measured at 20 °C to be between 2.05 and 2.1. Then the colloid solution was sonicated in an ultrasonic bath (5 × 1 min at 250 W) for 5 min. Finally, the amorphous TiO_2 nanoparticles were separated from the solvent by centrifugation at 5000 rpm for 15 min.

2.2. Transparent conductive substrates

SnO_2:F (FTO) plates (Solaronix, 10 Ω/□, TCO glasses, 1 mm thick) were used as transparent conductive substrates for deposition of TiO_2 semiconductor films. Since the microscope investigations of FTO films revealed some damage to the surface after cutting, the films were covered by photoresist (Shipley 1818) to protect the surface of the FTO film. The sprayed thick layer of photoresist was dried at room temperature for 2 h. The cut FTO glasses were cleaned by subsequent sonication in acetone, ethanol, Hellmanex (Hellma GmbH & Co.), then in deionized water and again in ethanol (for 15 min in each solvent). The cleaning in acetone easily removed the photoresist from the FTO surfaces as we did not use temperatures above 100 °C to make the photoresist firm. The cleaned substrates were kept in ethanol before use.

2.3. Dense nanocrystalline film deposition

The nanocrystalline TiO_2 films were deposited by a spray pyrolysis method, as described earlier [20]. The cleaned FTO substrates were dried in flowing nitrogen. Then the substrates were located on a hot-plate (Cimarec) and heated for 30 min at 510 °C before spraying. It is known that all organics from the films can be burned out by annealing them above 450 °C [20]. During the spraying procedure, a narrow part at the edge of the FTO was protected from the TiO_2 deposition by a FTO glass mask. Di-iso-propoxy titanium bis-(acetylacetonate) (TAA) was used as a source of titanium. The precursor was prepared by mixing 0.1 M of titanium tetra-isopropoxide (Sigma-Aldrich, 99.99%) and 1.2 M acetylacetone AcAc (Fluka, 99.9%) in ethanol. A chromatographic atomizer was used to spray layer-by-layer the solution of acetylacetonate onto the 510 °C heated substrates. Each portion of the precursor was sprayed after a pause of 20 s to complete the pyrolysis of the previous layer and to restore the initial substrate temperature. The deposited films were annealed at 500 °C for 30 min in the air to complete the crystallization of TiO_2 nanoparticles and remove the remaining organic traces.

2.4. Nanoporous electrode fabrication

The environment of the slurry was changed from pH 2.6 to 5 by adding 0.01–0.06 M NH_4OH (Riedel–de Haën, 33%) to every 10 g of the centrifuged acidic resultant. The TiO_2 slurry was carefully stirred and immediately printed by a doctor-blade technique on the substrates covered with the TiO_2 nanocrystalline dense films. Scotch Magic Tape with a thickness of 50 μm was used to provide contact areas on the FTO surface. After drying in the air for an hour, the films were gradually annealed: e.g. for annealing at 500 °C the program was first 75 °C for 15 min, then 150 °C for 15 min, afterward 300 °C for 10 min, and 500 °C for 15 min. The temperature was ramped up for 20 min at each step. The annealed TiO_2 electrodes were cooled down to room temperature and were then immersed into 0.5 mM D719 dye solution (Solaronix) made in acetonitrile (Echo, 99.98%) and *tert*-butanol (Fluka, 99%) 1:1 v/v solvent mixture. The electrodes were kept at room temperature for 4 days in the dark. After dye adsorption the color of the TiO_2 electrodes changed to a deep red. The colored electrodes were washed by acetonitrile from the excess dye solution and were held in absolute ethanol until the photovoltaic measurements.

2.5. Imaging, analysis and characterization

The crystallinity and the phase composition of the TiO_2 films were examined with Bruker-D8 x-ray powder diffractometer using Cu Kα radiation. The size of particles and the morphology of the TiO_2 film surface were studied with an AFM-D3100 atomic force microscope and a Hitachi S-4800 high resolution SEM. The thicknesses of TiO_2 films were measured by an XP-1 surface profiler. The surface areas of the TiO_2 photoelectrodes were measured by a Marscam microscope. The absorption spectra of the multilayer photoelectrodes were investigated with a Varian Cray 50 spectrometer. The current–voltage characteristics of the photoelectrodes and solar cells were measured using a Kethley 2440 sourcemeter. An AM1.5 solar simulator (YSS-50, Yamashita Denso) with a 1000 W Xe lamp was employed as the light source. A calibrated Si cell was used as a reference.

2.6. Solar cell assembly

The dye-adsorbed TiO_2 photoelectrodes and the Pt counter electrodes were assembled into sandwich-type cells. Counter electrodes were prepared by dropping H_2PtCl_6 (Sigma-Aldrich) solution on the FTO glass plates, drying in air for 10 min and heating at 400 °C for 15 min. A 60 μm thick polyethylene spacer was used to separate the TiO_2 electrode from the Pt counter electrode. The space between the electrodes was filled with a redox electrolyte consisting of 0.6 M 1-butyl-3-methyllimidazolium iodide (BMPImI; Merck), 0.1 M guanidinium thiocyanate $NH_2C(NH)NH_2$ (HSCN, Fluka, 99%), and 0.03 M I_2 (Riedel–de Haën) in acetonitrile (Echo, 99.98%) and valeronitrile v/v 4:1 (Sigma-Aldrich, 99.5%) with 0.5 M 4-*tert*-butylpyridine TBP (Sigma-Aldrich). The solar cell areas were 0.12–0.25 cm^2 in size.

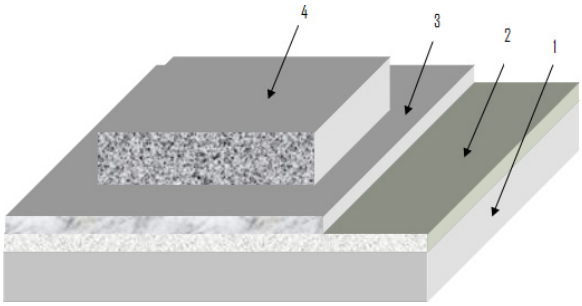

Figure 1. Multilayer structure of TiO_2 photoelectrodes: 1, glass; 2, SnO_2:F(FTO) film; 3, dense nanocrystalline TiO_2 film; 4, nanoporous TiO_2 film.

3. Results and discussion

The structure of the highly photoactive two-layer TiO_2 electrode is shown in figure 1. The electrode consists of FTO film deposited on glass and covered with nanocrystalline TiO_2 dense thin film followed by nanoporous TiO_2 thick film.

Microscope and AFM investigations of the FTO films revealed that a photoresistive layer did not remain on the FTO surfaces after the heating of glass substrates at 510 °C. We also found out that the dense TiO_2 films deposited on the FTO films were more homogeneous and compact, while the photoresist was used in a plate-cutting procedure. The photovoltaic measurements revealed that the more homogeneous and compact the deposited dense TiO_2 films, the better they prevent the liquid electrolyte from electrical connection with the FTO film. AFM images of the FTO film surfaces before and after deposition of the dense TiO_2 film are shown in figure 2. The FTO film consists of FTO collapses varying from 40 to 200 nm in diameter. These collapses are seen not to be packed densely into each other. Since the average thickness of the FTO films is 250–300 nm, only one or two layers of FTO collapses comprise the FTO films. The surface area difference (SAD), which is a parameter often used for characterizing the film surface in AFM image analyses [21], is described by the following expression:

$$\mathrm{SAD} = \left[\frac{\sum(\mathrm{SA})}{\sum(\mathrm{PA})} - 1\right] \times 100\% \qquad (1)$$

where SA is a three-dimensional surface area and PA is a two-dimensional surface area produced by projecting the three-dimensional surface onto the measured threshold plane. The AFM analyses of the images shown in figure 2 show that the average value of the SAD of the FTO films is 65%. This parameter decreases to 40% after deposition of the dense packed layer of TiO_2 nanoparticles on the FTO film.

The densely packed TiO_2 film was deposited on the FTO glass by a spray pyrolysis method, as described in section 2.3. XRD analysis of dense TiO_2 films shows formation of the anatase phase after final annealing of the films at 500 °C. Thin TiO_2 films are usually grown on the FTO glasses to prevent electrical connection of the liquid I^-/I_3^- redox electrolyte with n-doped FTO conductive electrodes. The maximum fill-factor for the solar energy conversion and the best reproducibility

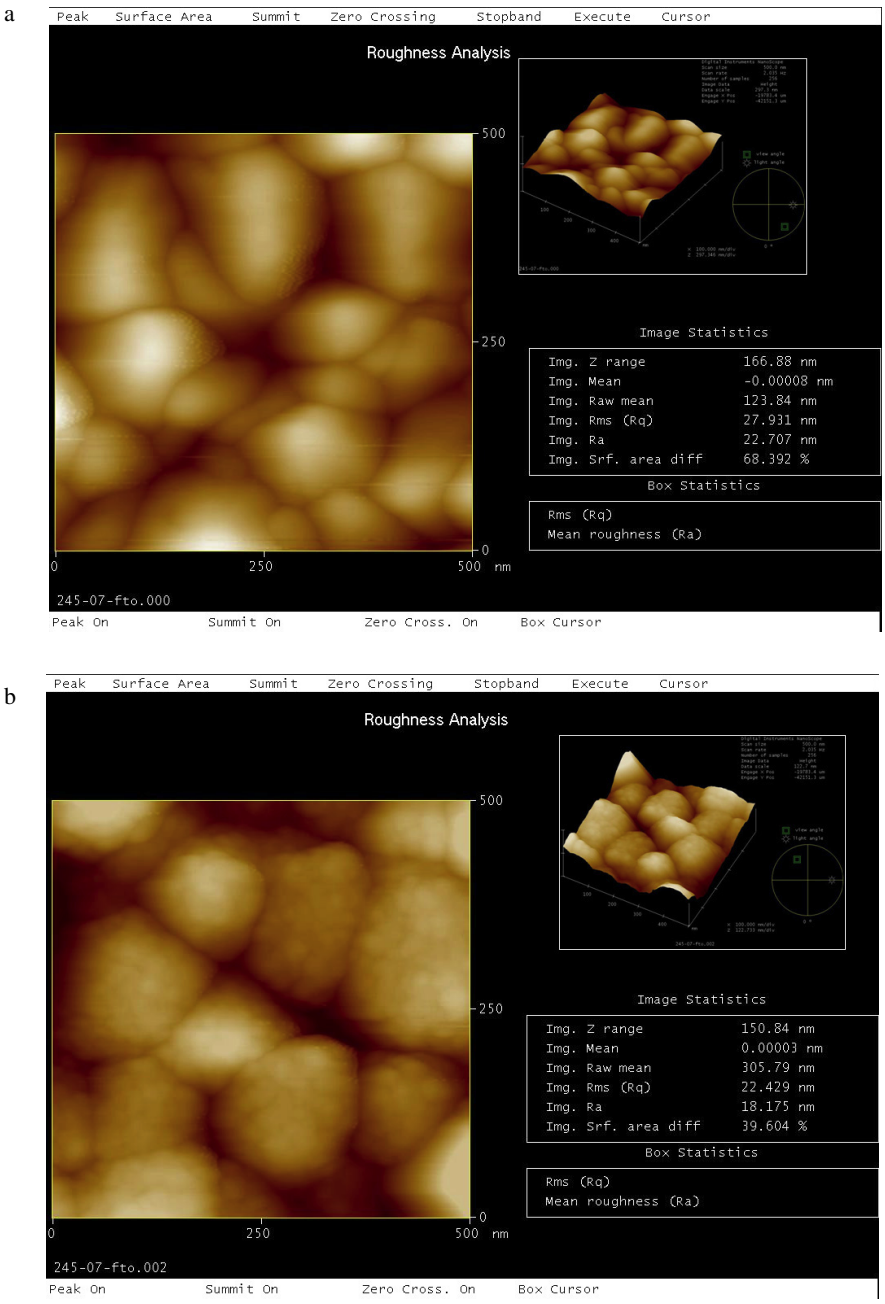

Figure 2. AFM images of the SnO_2:F (FTO) film (a) and SnO_2:F film covered with TiO_2 dense film (b). The TiO_2 dense film was deposited by five or six consecutive spraying cycles of the TAA solution on the FTO film, after which the heat treatment at 500 °C was followed for 30 min in air. The means converted to average values taken from four surveyed areas of the substrate are: (a) image raw mean 130 nm, Rms (Rq) 20 nm, Ra 20 nm, surface area difference 65%; (b) image raw mean 250 nm, Rms (Rq) 30 nm, Ra 20 nm, surface area difference 40%.

of the solar cells were obtained after five or six consecutive sprayings cycles of precursor. The average thickness of the dense TiO_2 films was 60–70 nm, measured by profiler. Further spraying decreased the transparency of the FTO films and spoiled the fill-factor of the cells. An AFM image of the FTO film, covered with the annealed dense TiO_2 film, is shown in figure 2(b). The AFM images of the FTO film surfaces reveal that the densely packed layer of TiO_2 nanoparticles fully covers the surface of the FTO collapses after five or six consecutive spraying cycles. The size of TiO_2 nanoparticles in the densely packed layer is seen to be approximately 20–30 nm. It is assumed that only two or three layers of the TiO_2 nanoparticles comprise the densely packed layer since the average thickness of the densely packed layer is 60–70 nm. Comparing the AFM images in figures 2(a) and (b), one can reveal that the FTO films consist of large and small FTO collapses and that the small FTO collapses disappear after the deposition of the TiO_2 nanoparticles. Evidently the deposited TiO_2 nanoparticles fill the small wells between small and large FTO collapses. Therefore, the film surface becomes flat at the grain boundaries

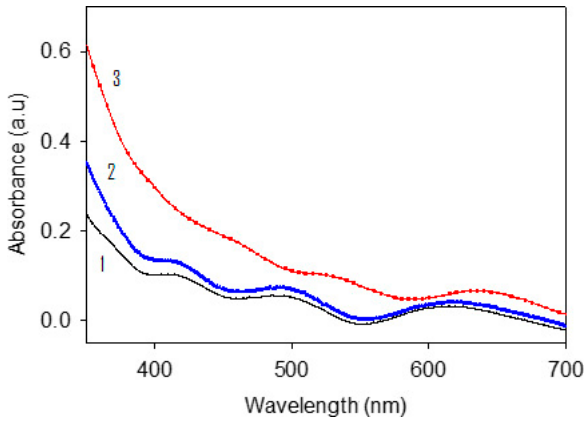

Figure 3. Optical absorption spectra of FTO film and nanocrystalline TiO_2 films: black (1) curve, FTO film; blue (2) curve, nanoporous TiO_2 film coated on the dense TiO_2 film deposited on the FTO: red (3) curve, FTO film covered with the dense nanocrystalline TiO_2 thin film;

between the small and large FTO collapses and the surface area difference of the FTO glass substrate decreases from 65% to 40% after the deposition of the dense TiO_2 film.

The nanoporous thick TiO_2 films were fabricated from the colloid of TiO_2 nanoparticles synthesized by the sol–gel method described in section 2. The average size of the TiO_2 nanoparticles is 20 nm in the colloid when the hydrothermal growth temperature is 200 °C and the pH of the sol is 0.95–0.98. This combination of autoclaving parameters used for synthesizing the TiO_2 gel was found to be crucial for fabrication of transparent and reproducible nanoporous TiO_2 films. The centrifuged initial resultant of the TiO_2 gel had a pH of 2.1. The pH of the final resultants used for deposition of nanoporous thick TiO_2 films varied from 2.62 to 5.01 by adding basic ammonia to the initial acidic resultants.

Figure 3 displays the absorption spectrum of the FTO glass substrates. The transparency of the substrates is seen to be reduced a little after covering with a densely packed nanocrystalline TiO_2 layer. Nevertheless, the next deposition of the nanoporous thick TiO_2 film on the dense film is seen to be restoring the transparency. This effect is reproducible, although the reduction in the transparency is very small for some samples. The reduction in the transparency can be attributed to the additional reflection from the interface between the densely packed layer and the air. The AFM images in figure 2 show that the densely packed TiO_2 thin layer smooths the film surface at the grain boundaries between the small and large FTO collapses. Coating the pH 5 gel with the dense TiO_2 film is expected to introduce discharged TiO_2 nanoparticles into the large wells between large FTO collapses. The discharged TiO_2 nanoparticles stick better to the densely packed nanocrystalline TiO_2 layer and smooth the FTO film surface at the grain boundaries between large FTO collapses. Filling large wells between large FTO collapses should restore the transparency of the FTO glass substrates. We also observed that after the deposition of the dense and nanoporous TiO_2 films the low-transparent lusterless FTO glass substrates became even more transparent than the initial FTO substrates.

The most viscous anatase TiO_2 slurry has a pH of 6.2 [17, 19]. We investigated nanoporous thick TiO_2 films prepared from the colloidal resultants with pH 2.1, 2.6, 3.5, 3.85, 4.5 and 5, respectively. Initially, the centrifuged resultant of the TiO_2 gel used for film deposition had a pH of 2.1. By adding 0.005–0.06 M 33% NH_4OH to the initial resultants, the pH of the resultants was varied from 2.62 to 5.01. The maximum pH achieved was 5.01, as further addition of NH_4OH did not significantly change the pH of the centrifuged resultants and we did not reach pH 6.2 of the most viscous anatase TiO_2 slurry [17, 19].

The SEM and AFM images of the nanoporous TiO_2 films show that ammonia induces the formation of nanoporous films divided by 'channels' into 'blocks' as shown in figures 4(a) and 5(d). The formation of 'blocks' and 'channels' had been also reported by Hart *et al* [22]. We found that the films fabricated from almost ammonia-free TiO_2 slurry, pH $<$ 2.6, were uniform and did not have any 'channels' or 'blocks' as shown in figure 5(a). The film shown in figure 5(a) was annealed by a standard heating program (75 °C for 15 min, at 150 °C for 15 min, at 300 °C for 15 min and at 500 °C for 15 min in the air). The temperature was ramped up for 20 min at each step of this standard heating program. The same morphology shown in figure 5(a) had films fabricated from the same slurry, pH $<$ 2.6, and annealed for a longer time at 350 °C or higher temperatures. Furthermore, the films fabricated from the TiO_2 slurry with added ammonia, pH $>$ 2.6, and annealed by the same standard heating program or at 350 °C and higher temperatures were divided by 'channels' into 'blocks' shown in figures 4(a) and 5(d). Figure 5(d) exhibits an essentially different structure of the 'channels' and 'blocks'. This film was fabricated from the TiO_2 slurry with excess ammonia and annealed by a standard heating program.

The films fabricated from the TiO_2 slurry with added ammonia, pH $>$ 2.6, annealed by the heating program at 100 °C for 15 min, at 150 °C for 15 min and at 300 °C for 15 min in the air, had no 'channels' and 'blocks' and looked like the film shown in figure 5(a). However, formation of 'channels' and 'blocks' appeared when these films were annealed for longer at 300 °C or at lower temperatures. For instance, figure 5(b) exhibits the morphology of the film fabricated from the slurry with pH 5 and annealed at 300 °C for 60 min, and figure 5(c) exhibits the morphology of the film fabricated from the slurry with pH 5 and annealed at 250 °C for 240 min. Hence, the formation of the 'channels' and 'blocks' does not strongly depend on the annealing regime of the films. However, it evidently depends on the presence of ammonia in the gel. Thus, the simultaneous occurrence of partially discharged and positively charged nanoparticles can bring about the formation of such films during the crystallization.

The SEM image of the 'channeled' nanoporous TiO_2 film is shown in figure 4. The 'blocks' seem to be separated from each other by 'channels', as shown in figures 4(a) and (b). Under the higher resolution displayed in figures 4(c)–(e), the SEM analysis reveals that nanoparticles also fill the 'channels' between the 'blocks'. Nevertheless, the density of these nanoparticles placed within the 'channels' is abruptly reduced at the edge of the 'blocks'. The reduction in the density is so

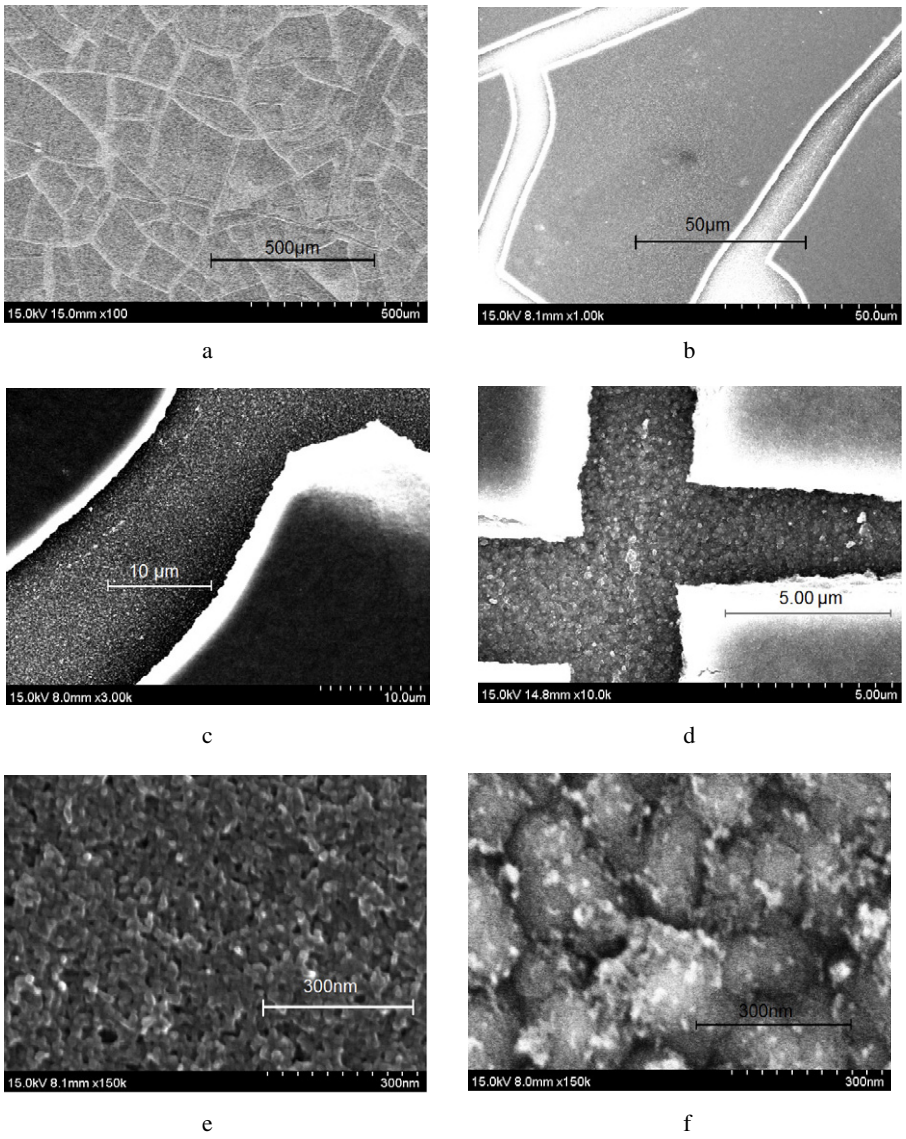

Figure 4. SEM images of nanoporous TiO_2 film surfaces prepared from TiO_2 gel, pH 5.0, annealed consequently at 100 °C for 15 min, at 150 °C for 15 min, at 300 °C for 15 and at 500 °C for 15 min in air: (a) the image of the film surface; (b)–(d) the images of the 'channels'; (e), (f) the images of nanoparticles in the 'channels' (a similar image has nanoparticles in the 'blocks').

abrupt that the nanocrystalline TiO_2 dense thin film covering the FTO collapses is clearly seen in the 'channels' shown in the figure 4(f). This picture demonstrates how important the growth of the dense films on the conductive substrate is. In the 'channels' the liquid conducting electrolyte is separated from the FTO film at least by the dense film. Therefore, the dense film of TiO_2 nanoparticles must be well packed and have no porosity to avoiding current leakage and short-circuiting in the cells.

Analyzing the AFM images of the nanoporous TiO_2 films it is observed that the SADs are increased along with increase in the annealing temperature of the films above 350 °C and the amount of ammonia in the colloids. It is noteworthy that the AFM analyses reveal that the SADs in the 'channels' are approximately the same as in the 'blocks' shown in figure 6.

XRD analysis was used to determine the crystal structure and the phase formation of the samples. Figure 7 shows significant differences in intensities of the XRD diffraction peaks of the nanocrystalline films fabricated with and without ammonia under the same annealing conditions. The intensity of the TiO_2 anatase peaks is approximately the same for the films with added ammonia annealed at 150 °C for 1 h, 250 °C for 3 h, and the ammonia-free films annealed at 500 °C for 15 min. However, the intensity of the peaks is seen to be significantly increased for the films with added ammonia annealed at 500 °C for 15 min. The increased intensity of the peaks can be attributed to the co-orientation of the nanocrystallites in the films annealed at higher temperatures. Since the discharged nanoparticles are in better contact with each other, the nanocrystallites heated up to 500 °C can gain the interface strain energy by adjusting the orientation of nanocrystallites and creating dislocation-free interfaces. Therefore, the electrons generated in the conduction band of the ammonia-based films fabricated at 500 °C can easily

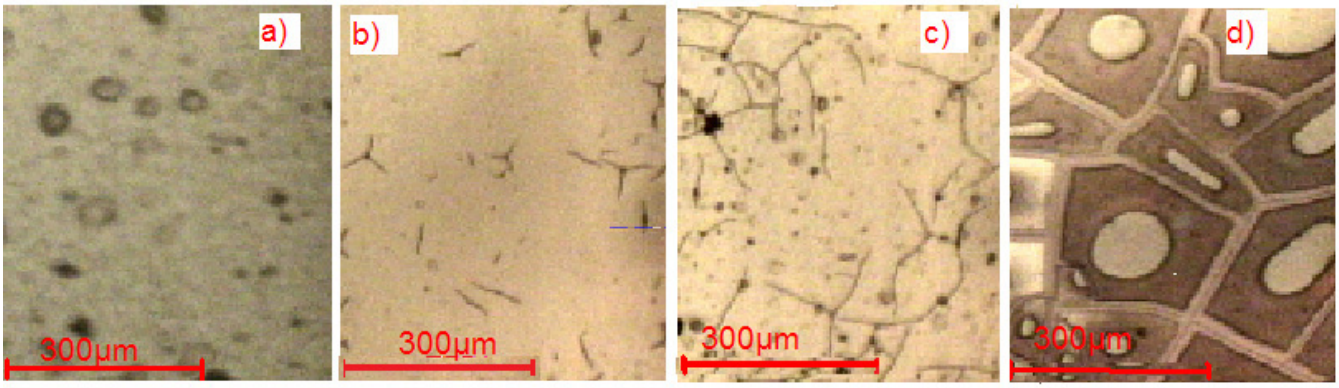

Figure 5. AFM images of nanoporous films prepared from TiO_2 gel with different pHs and subsequently annealed by different heating programs: the temperature was ramped up for 20 min at each step of following heating programs. (a) pH 2.6, heating program 75 °C for 15 min, 150 °C for 15 min, 300 °C for 15 and 500 °C for 15 min; (b) pH 4.5, heating program 100 °C for 15 min, at 150 °C for 15 min and at 300 °C for 60 min; (c) pH 4.5, heating program 100 °C for 15 min, at 150 °C for 15 min and at 250 °C for 240 min; (d) pH 5 with an additional amount of ammonia heated by the program 75 °C for 15 min, 150 °C for 15 min, 300 °C for 15 and 500 °C for 15 min.

pass through the interfaces between nanocrystallites. This could why higher photoactivity is achieved in discharged nanocrystallites annealed at higher temperatures.

The photovoltaic measurements were carried out for a few hundred samples. Since these characteristics depend on the amount of ammonia in the slurry and on photoactive surface areas as well as on the thickness of the nanoporous films, we separated the data obtained for samples that have approximately the same photoactive surface areas and the same nanoporous film thickness. The dependence of conversion efficiency and photocurrent density on the annealing temperature was investigated on the basis of these data. Figure 8 displays these dependences for approximately 5 μm thick films with 0.12–0.14 cm^2 active surface areas fabricated by a one-coating procedure. The dependences obtained for the films fabricated from the TiO_2 colloid with added ammonia, pH 5, and that from the ammonia-free TiO_2 colloid, pH 2.1, are also compared with each other in figure 8. Each point in figure 8 represents the averaged data obtained from 10–20 samples. The standard variation of each point is approximately 15% of its value. Figure 8 reveals that the photocurrents and the conversion efficiencies of both ammonia-free and ammonia-added cells increase almost linearly with increase in the annealing temperature from 150 to 500 °C. The slope of the lines is clearly seen to be larger for the cells with added ammonia. The increased slope correlates with AFM and SEM images which reveal the formation of a 'channeled' morphology in the films with added ammonia. No abrupt change triggered with the annealing temperature is seen in the structure of the films. Instead, the slow formation of the 'channeled' morphology was initiated at lower annealing temperatures, while for temperatures above 350 °C complete 'channeled' films were rapidly formed. We attributed the linear increase in the photocurrents and conversion efficiencies to improvement of the co-orientation and interconnection of nanocrystallites along with annealing of the films in the presence of ammonia. The improvement must also be attributed to the 'channeled' morphology of the nanoporous TiO_2 films. The increased photocurrents may imply that the 'channels' support better penetration and more absorption of dye molecules into 'blocks', as considered by Hart *et al* [22]. However, no essential color changes have been found among the samples annealed at different temperatures. Therefore, the improvement in efficiency can be associated with better penetration of dye molecules in the spaces between the dense and nanoporous TiO_2 films. Since the dense TiO_2 films actually create extremely narrow molecular pores, the dye molecules may, to some extent, be able to seal the molecular pores and suppress the current leakage through the molecular pores of the nanocrystalline TiO_2 dense thin films. AFM analysis of the nanoporous TiO_2 film surfaces also supported the suggestion concerning the sealing of the molecular pores. In most cases the SADs (1) were seen to be significantly increased (about twice) by adding ammonia. Obviously, the higher the roughness at the interface between the dense and nanoporous TiO_2 films, the better the dye molecules may penetrate into the space between the dense and nanoporous TiO_2 films and seal the molecular pores of the dense TiO_2 layers.

Figure 9 displays the current–voltage characteristics of DSSC based on the nanoporous TiO_2 films. It is seen that fabrication with ammonia promotes an improvement in the performance of the cells. The highest conversion efficiency of 8.83% was exhibited by the cells incorporated into the 'channeled' nanoporous 13 μm thick films fabricated from the colloid with pH 5. The cell area, the fill-factor, the open-circuit voltage, and the short-circuit current were 0.12 cm^2, 69.2%, 793 mV, and 16.1 mA cm^{-2}, respectively. For comparison, figure 8 also displays the current–voltage characteristics of the cells incorporated into the ammonia-free nanoporous 18 μm-thick films fabricated from the same initial colloid. The highest conversion efficiency in these cells was 6.61% while the cell area, the fill-factor, the open-circuit voltage, and the short-circuit current were 0.2 cm^2, 66.2%, 819 mV, and 12.2 mA cm^{-2}, respectively.

Understanding the factors that control parameters like photocurrent, photovoltage, dark current, fill-factor and conversion efficiency of DSSCs is an important topic for

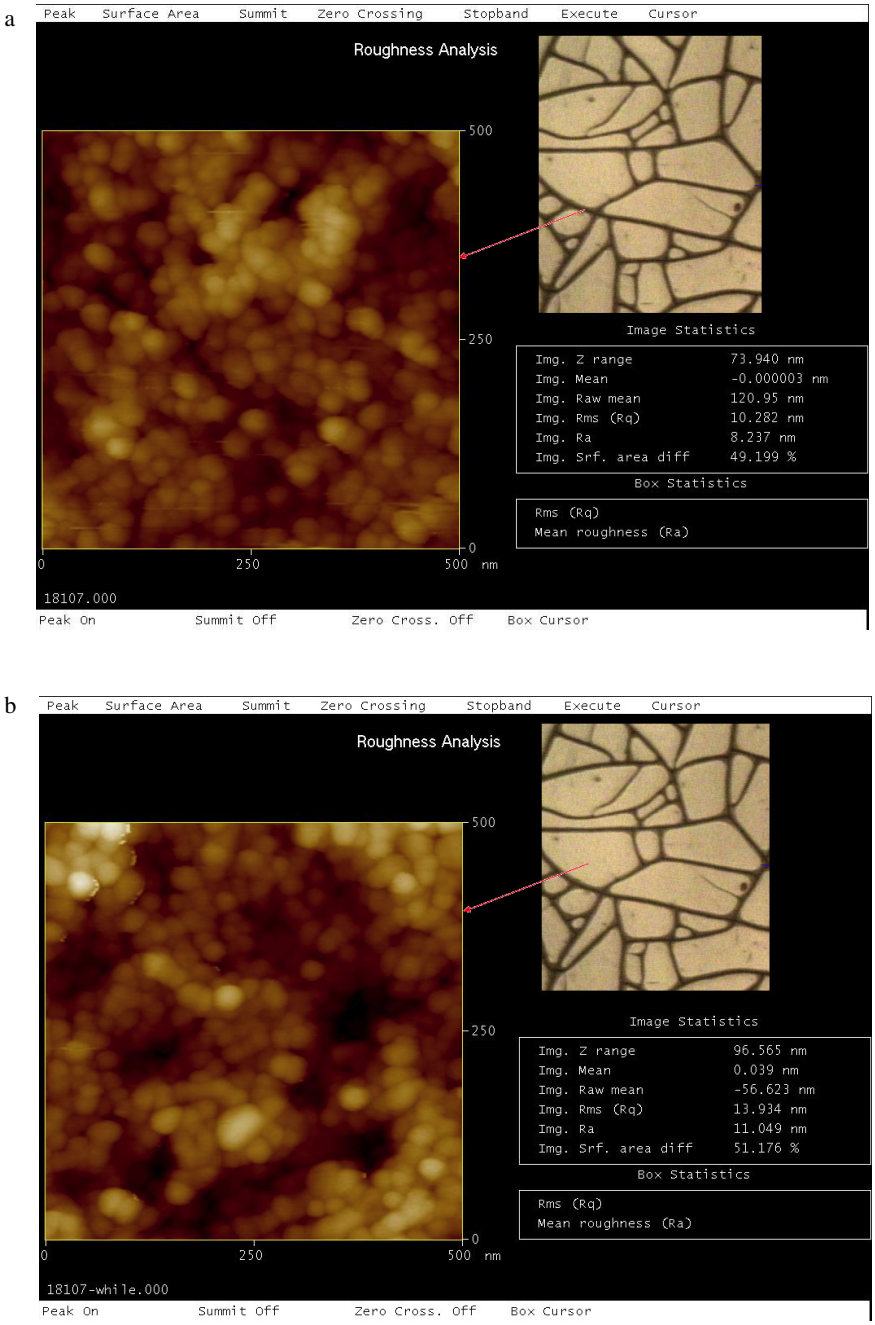

Figure 6. AFM images of nanoporous film prepared from TiO_2 gel, pH 4.5, annealed subsequently at 100 °C for 15 min, at 150 °C for 15 min, at 300 °C for 15 and at 500 °C for 15 min in the air: (a) the scan of the 'channel' area: Rms (Rq) 10 nm; Ra 8 nm; surface area difference 50%; (b) the scan of the block area: Rms (Rq) 14 nm; Ra 11 nm; surface area difference 51%; (c) the image of the film surface.

future studies. The data displayed in figures 7 and 8 show that adding ammonia to the TiO_2 slurry increases the overall conversion efficiency of DSSCs by approximately 30%, while the pH of the slurry was increased from 2.6 to 5.01. The increase in efficiency is associated with better interconnection of nanoparticles in the nanoporous TiO_2 films, higher homogeneity of pores and better separation of liquid electrolyte from FTO film. We have already achieved a conversion efficiency of 8.83% in the most efficient cell, although the proposed method has not been completely optimized yet. As already mentioned, the TiO_2 slurry is most viscous at pH 6.2 [17, 19]. We have already achieved pH 5 and are trying to get closer to pH 6.2. It is supposed that the more viscous the slurry is, the better the interconnection of nanoparticles and the higher the homogeneity of pores in nanoporous TiO_2 films. Therefore, more dye can be absorbed and higher photocurrent can be generated in cells fabricated from the most viscous TiO_2 slurry. We also found that the densely packed layer of TiO_2 nanoparticles deposited by spraying for more than five or six times decreased the fill-factor and the photocurrent of the cells. Therefore, fabrication of dense films with lower thickness can improve the efficiency

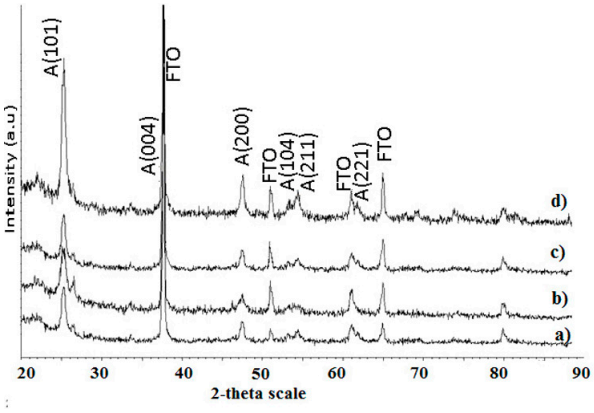

Figure 7. X-ray diffraction patterns of TiO_2 nanocrystalline film deposited on FTO substrates. FTO peaks also appeared on the diffraction peaks. (a) TiO_2 film prepared from the ammonia-free colloid with pH 2.1, followed by heat treatment at 500 °C for 15 min; (b)–(d) TiO_2 films prepared from the ammonia-added colloid with pH 5.0, followed by heat treatment at 150 °C for 60 min, at 250 °C for 180 min, at 500 °C for 15 min, respectively.

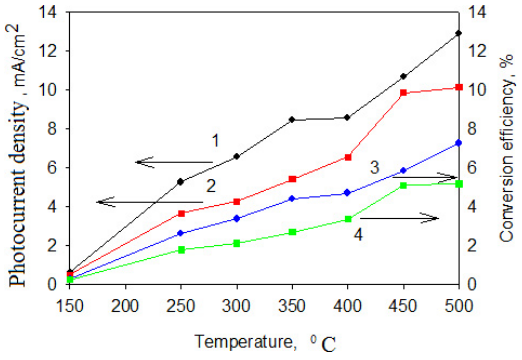

Figure 8. The photocurrent density (1 and 2) and the conversion efficiency (3 and 4) of the nanocrystalline TiO_2 films prepared from the colloids with pH 2.1 (2 and 4) and pH 5.0 (1 and 3) as the function of the annealing temperature.

of cells. Our aim is to improve the deposition of dense films to achieve more homogeneity and better packed thinner films by decreasing the size of nanoparticles.

4. Conclusion

In summary, using an easy and a cheap technique we have been able to fabricate highly active transparent conductive nanocrystalline TiO_2 photoelectrodes from discharged nanoparticles.

We have shown that the nanoporous nanocrystalline TiO_2 films fabricated with ammonia improve the performance of DSSCs. SEM, AFM and XRD analyses revealed a significant difference in both surface morphology and crystal structure of ammonia-based and ammonia-free mesoporous TiO_2 films. The conversion efficiency of these DSSCs was increased from 6.61% to 8.83% along with increasing pH of the TiO_2 binder-free acidic colloid from 2.1 to 5 and modification of the surface morphology. Analyses of the photocurrent–voltage characteristics revealed that the improved performance was associated with better interconnection and co-orientation of

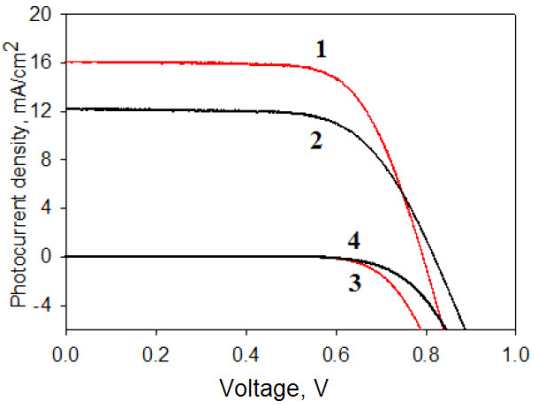

Figure 9. Photocurrent (1and 2) and dark current (3 and 4) current–voltage characteristics of DSSC cells based on nanoporous TiO_2 film fabricated from (1, 3) ammonia-added colloid with pH 5.0 and (2, 4) ammonia-free colloid with pH 2.1.

nanocrystallites in the films fabricated with ammonia. The proposed method simplifies the technique for fabricating the photoelectrodes by avoiding some standard procedures such as adding the binder, treating the nanoporous TiO_2 surfaces, and immersing the hot electrodes into the dye.

Acknowledgments

This work was financially supported by 952001INER027 and 962001INER0029 Solar Energy Projects of Taiwan. The authors thank to C K Wang for x-ray patterns, T T Wang for SEM images and J L Liu for organization of AFM measurements. The authors also thank Dr G Badalyan for discussions.

References

[1] O'Regan B and Gratzel M 1991 A low-cost, high efficiency solar cell based on dye-sensitized colloidal TiO_2 films *Nature* **353** 737–40

[2] Kalyanasundaram K and Gratzel M 1998 Application of functionalized transition metal complexes in photonic and optoelectronic devices *Coord. Chem. Rev.* **77** 347–414

[3] Zaban A, Micic O I, Gregg B A and Nozik A J 1998 Photosensitization of Nanoporous TiO_2 Electrodes with InP quantum dots *Langmuir* **14** 3153–6

[4] Yu P, Zhu K, Norman A G, Ferrere S, Frank A J and Nozik A J 2006 Nanocrystalline TiO_2 solar cells sensitized with InAs quantum dots *J. Phys. Chem.* B **110** 25451–4

[5] Zaban A, Ferrere S, Sprague J and Gregg B A 1997 pH-dependent redox potential induced in a sensitizing dye by adsorption onto TiO_2 *J. Phys. Chem.* B **101** 55–7

[6] Nazeeruddin M K, Kay A, Rodicio I, Humphry-Baker R, Muller E, Liska P, Vlachopoulos N and Gratzel M 1993 Conversion of light to electricity by *cis*-X2bis(2, 2′-bipyridyl-4, 4′-dicarboxylate) ruthenium(II) charge-transfer sensitizers (X = Cl-, Br-, I-, CN-, and SCN-) on nanocrystalline titanium dioxide electrodes *J. Am. Chem. Soc.* **115** 6382–90

[7] Park N-G, Schlichthöt G, van de Lagemat J, Cheong H M, Mascarenhas A and Frank A J 1999 Dye-Sensitized TiO_2 solar cells: structural and photoelectrochemical

characterization of nanocrystalline electrodes formed from the hydrolysis of $TiCl_4$ *J. Phys. Chem.* B **103** 3308–14
[8] Barbe C, Arendse F, Comte P, Jirousek M, Lenzmann F, Shklover V and Gratzel M 1997 Nanocrystalline titanium oxide electrodes for photovoltaic applications *J. Am. Ceram. Soc.* **80** 3157–71
[9] Nazeeruddin M *et al* 2001 Engineering of efficient panchromatic sensitizers for nanocrystalline TiO_2-based solar cells *J. Am. Chem. Soc.* **123** 1613–24
[10] Burnside S, Shklover V, Barbe C, Comte P, Arendse F, Brooks K and Gratzel M 1998 Self-organization of TiO_2 nanoparticles in thin films *Chem. Mater.* **10** 2419–25
[11] Sugimoto T, Zhou X and Muramatsu A 2002 Synthesis of uniform anatase TiO_2 nanoparticles by gel–sol method: 1. solution chemistry of $Ti(OH)_n^{(4-n)+}$ complexes *J. Colloid Interface Sci.* **252** 339–46
[12] Sugimoto T and Zhou X 2002 Synthesis of uniform anatase TiO_2 nanoparticles by the gel–sol method: 2. adsorption of OH^- Ions to $Ti(OH)_4$ Gel and TiO_2 particles *J. Colloid Interface Sci.* **252** 347–53
[13] Sugimoto T and Zhou X 2003 Synthesis of uniform anatase TiO_2 nanoparticles by gel–sol method: 3. Formation process and size control *J. Colloid Interface Sci.* **259** 43–52
[14] Gratzel M 2001 Sol–gel processed TiO_2 films for photovoltaic applications *J. Sol-Gel Sci. Technol.* **22** 7–13
[15] Gratzel M 1999 Mesoporous oxide junctions and nanostructured solar cells *Curr. Opin. Colloid Interface Sci.* **4** 314–21
[16] Kavan L, O' Regan B, Kay A and Gratzel M 1993 Preparation of TiO_2 (anatase) films on electrodes by anodic oxidative hydrolysis of $TiCl_3$ *J. Electroanal. Chem.* **346** 291
[17] Larson R G 1999 *The Structure and Rheology of Complex Fluids* (New York: Oxford University Press)
[18] Park N G, Kim K M, Kung M G, Ryu K S, Chang S H and Shin Y J 2005 Chemical sintering of nanoparticles: a methodology for low-temperature fabrication of dye-sensitized TiO_2 films *Adv. Mater.* **17** 2349–53
[19] Parks G A 1965 The isoelectric points of solid oxides, solid hydroxides, and aqueous hydroxo complex systems *Chem. Rev.* **65** 177–98
[20] Kavan L and Gratzel M 1995 Highly efficient semiconducting TiO_2 photoelectrodes prepared by aerosol pyrolysis *Electrochim. Acta* **40** 643–52
[21] Russ J C (ed) 1992 *Computer-Assisted Microscopy. The Measurement and Analysis of Images* (New York: Plenum) p 450
[22] Hart J N, Menzies D, Cheng Y B, Simon G P and Spiccia L 2007 A comparison of microwave and conventional heat treatments of nanocrystalline TiO_2 *Sol. Energy Mater. Sol. Cells* **91** 6–16